The Design of Serpentine-Mode Converters for High-Power Microwave Applications

Wes Lawson, *Senior Member, IEEE*, Melany R. Arjona, Bart P. Hogan, and R. L. Ives, *Senior Member, IEEE*

***Abstract*—In this paper, we report the design methodology and numerical results for two mode converters that are suitable for high-power microwave applications. Both converters are designed to operate at 11.424 GHz and utilize periodic serpentine structures to convert between modes with different azimuthal-mode indexes. The first converts about 98.5% of an incident linearly polarized TE_{12} mode to the TE_{01} mode when oriented as an H-plane bend, but has just 1% mode conversion to all modes when oriented as an E-plane bend. The second device converts a linearly polarized TE_{11} mode to a TM_{01} mode with over 99.99% effectiveness. The performance of both devices with respect to parametric variations is detailed. Experimental measurements of the radiation patterns from the TE_{12}-to-TE_{01}-mode converter are consistent with the theoretical predictions.**

***Index Terms*—Microwaves, mode converter, overmoded circular waveguide.**

I. Introduction

THERE ARE many applications in high-power microwave (HPM) systems for components that convert between various mode patterns in overmoded waveguides. One application occurs whenever the mode that is produced in an HPM tube differs from the mode that needs to be transported or delivered to the load. For example, high-power gyrotron oscillators typically produce output in circularly polarized modes (in circular or coaxial waveguides) with very large azimuthal-mode numbers and large radial-mode numbers, but the output window and transport system require a Gaussian-like mode [1]. As a second example, a TE_{01} mode is often desirable for long transmission lines and certain types of pulse-compression schemes [2] because of its low-loss properties. However, the TE_{01} mode is typically the output mode only for moderate power fast wave devices; all other tubes would require some mode converter. As a final example, a recent novel power distribution scheme for linear colliders requires mode transducers from linearly polarized TE_{12} modes to the TE_{01} mode [3].

The geometry of the mode converter that is required depends on the details of the two modes that are being interchanged. If the input and output modes are in circular waveguide and have the same azimuthal-mode index and the converter is simply exchanging radial-mode numbers, then the converter is axisymmetric [4]–[6]. If the difference in azimuthal-mode numbers between the input and output modes is one and the modes are linearly polarized, serpentine-mode converters can be utilized [6]–[9]. If the modes are circularly polarized, fluted waveguides can be used to convert between modes with different azimuthal-mode numbers [1]. For all types of mode converters, the profile of the waveguide variation is often sinusoidal, with the axial periodicity determined by the difference in the axial wavelengths between the two modes. With a sufficient number of periods, nearly complete mode conversion can be obtained between the desired modes, with virtually no mode conversion for other modes that may be injected into the converter. Nonperiodic variations can often be used to reduce the length of the converter [9], but in these devices, virtually all modes may experience significant mode conversion.

In this paper, we detail the design procedure and results for two periodic serpentine converters that are of interest for recent high-power applications. In Section II, we summarize the coupling equations for converters both when the transverse electric field is polarized perpendicular to the plane in which the waveguide center line lies (H-plane bend) and when the transverse electric field is polarized parallel to the plane in which the waveguide center line lies (E-plane bend). The first design is for a converter between a linearly polarized TE_{12} mode and TE_{01} mode. When one polarization of the TE_{12} mode enters the converter, it should be completely transformed into the TE_{01} mode. However, when the TE_{12}-mode polarization is rotated by 90°, the mode should pass through the converter unchanged. This design is discussed in Section III, along with the design of a $\mathrm{TE}_{11} \rightarrow \mathrm{TM}_{01}$-mode converter. In Section IV, we present experimental measurements of the $\mathrm{TE}_{12} \rightarrow \mathrm{TE}_{01}$-mode converter. We summarize the results of this effort in Section V.

II. Design Method

The method of simulating mode conversion in a serpentine converter is outlined in [4] and is based on the coupling equations specified in [7]. The converter geometry is shown in Fig. 1. The cross section of the pipe is circular with a constant radius of a. The center line of the waveguide lies in the $\hat{x}$–$\hat{z}$ plane and the formula for its displacement from the $\hat{z}$ axis is

$$s(z) = d \sin(2\pi z/\lambda_b). \tag{1}$$

The number of waveguide periods is N. If we write the amplitudes of the waves traveling in the forward ($+\hat{z}$) and reverse ($-\hat{z}$) directions in the converter as a vector

$$\vec{A} = \left(A_1^+, \cdots, A_n^+, A_1^-, \cdots, A_n^-\right) \tag{2}$$

where A_1^+ represents the first forward wave, A_1^- represents the first backward wave, etc., then the differential equation

Manuscript received February 26, 1999. This work was supported by the Department of Energy, and by Calabazas Creek Research.

W. Lawson, M. R. Arjona, and B. P. Hogan are with the Institute for Plasma Research, Electrical Engineering Department, University of Maryland at College Park, College Park, MD 20742 USA.

R. L. Ives is with Calabazas Creek Research, Saratoga, CA 95070 USA.

Publisher Item Identifier S 0018-9480(00)03765-0.

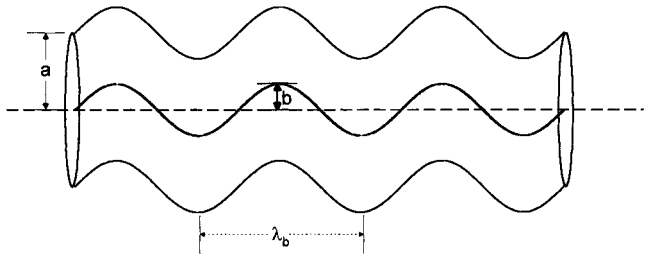

Fig. 1. Geometry of the serpentine converter.

that describes the evolution of the wave amplitudes with axial location is given by

$$\frac{d\vec{A}}{dz} = \left(\overleftrightarrow{\kappa} - \overleftrightarrow{\gamma}\right) \cdot \vec{A}. \tag{3}$$

The $\overleftrightarrow{\gamma}$ matrix is a diagonal matrix of axial wavenumbers

$$\overleftrightarrow{\gamma} = \mathrm{diag}\left(ik_1, \cdots, ik_n, ik_1, \cdots, -ik_n\right). \tag{4}$$

The elements of the coupling matrix $\overleftrightarrow{\kappa}$ are dependent on the specific modes (TE_{lm} or TM_{np}), whether the (electric) fields are polarized parallel or perpendicular to the plane of the center-line bend, and whether they are traveling in the forward or reverse directions. In the remainder of this section, we will use brackets $[lm]$ to denote a TE_{lm} mode and parentheses (np) to denote a TM_{np} mode.

The fields for TE modes are given by the generating function

$$\begin{Bmatrix} T^{\perp}_{[lm]} \\ T^{\parallel}_{[lm]} \end{Bmatrix} = \left[\frac{\varepsilon_l}{(x'^2_{lm} - l^2)\pi}\right]^{1/2} \frac{J_l(x'_{lm}r/a)}{J_l(x'_{lm})} \begin{Bmatrix} \cos(l\varphi) \\ \sin(l\varphi) \end{Bmatrix} \tag{5}$$

where the cosine dependence is for the H-plane bend and the sine dependence is for the E-plane bend. Note that we denoted the H-plane mode with the perpendicular sign ($\perp$) and the E-plane mode with the parallel ($\parallel$) sign. The usual Bessel function of the first kind is denoted $J_l(x)$, x'_{lm} is the mth zero of $J'_l(x)$, and $\varepsilon_l = 2$ if $l > 0$ and $\varepsilon_l = 1$ if $l = 0$. The normalized transverse magnetic fields ($\vec{b}_{[lm]}$) and electric fields ($\vec{e}_{[lm]}$) are given by

$$\vec{b}_{[lm]} = -\vec{\nabla} T_{[lm]} \quad \text{and} \quad \vec{e}_{[lm]} = -\hat{z} \times \vec{b}_{[lm]}. \tag{6}$$

The fields for TM modes are given by the generating function

$$\begin{Bmatrix} T^{\perp}_{(np)} \\ T^{\parallel}_{(np)} \end{Bmatrix} = i\left[\frac{\varepsilon_n}{\pi}\right]^{1/2} \frac{J_n(x_{np}r/a)}{x_{np}J_{n-1}(x_{np})} \begin{Bmatrix} \sin(n\varphi) \\ \cos(n\varphi) \end{Bmatrix} \tag{7}$$

where the sine dependence is now for the H-plane bend and the cosine dependence is for the E-plane bend. The pth zero of $J_n(x)$ is given by x_{np}. The normalized transverse electric fields ($\vec{e}_{(np)}$) and magnetic fields ($\vec{b}_{(np)}$) are given by

$$\vec{e}_{(np)} = -\vec{\nabla} T_{(np)} \quad \text{and} \quad \vec{b}_{(np)} = \hat{z} \times \vec{e}_{(np)}. \tag{8}$$

From (5)–(8), we see that the magnetic field at $\varphi = 0$ lies in the $\hat{x}$–$\hat{z}$ plane for both TE and TM perpendicular modes; hence, the name "H-plane bend." The circular electric modes (TE_{0m}) simply have the φ dependence replaced by unity in either polarization, but it turns out that there is no mode coupling between any parallel mode and any circular electric mode. Likewise, it turns out that TM_{0m} modes do not couple to perpendicular modes. Finally, there is no coupling whatsoever between any perpendicular mode and any parallel mode. For two perpendicular modes or two parallel modes, there is coupling only when the azimuthal mode indexes between the two modes differ by exactly one. For modes where coupling exists, the coupling coefficients are given by the following equations [7]:

TE $\rightarrow$ TE

$$\kappa^{\pm}_{[lm][np]} = \frac{-i}{2}\left(\frac{k^2\Xi_{[lm][np]} - x'_{lm}x'_{np}\xi_{[lm][np]}}{\sqrt{k_{lm}k_{np}}} \pm \Xi_{[lm][np]}\sqrt{k_{lm}k_{np}}\right) \tag{9}$$

TM $\rightarrow$ TM

$$\kappa^{\pm}_{(lm)(np)} = \frac{-i}{2}\left(\Xi_{(lm)(n-p)}\sqrt{k_{lm}k_{np}} \pm \frac{k^2\Xi_{(lm)(np)} - x_{lm}x_{np}\xi_{(lm)(np)}}{\sqrt{k_{lm}k_{np}}}\right) \tag{10}$$

TM $\rightarrow$ TE

$$\kappa^{\pm}_{[lm](np)} = -\frac{1}{2}k\Xi_{[lm](np)}\left(\sqrt{k_{np}/k_{lm}} \pm \sqrt{k_{lm}/k_{np}}\right) \tag{11}$$

TE $\rightarrow$ TM

$$\kappa^{\pm}_{(lm)[np]} = \frac{1}{2}k\Xi_{(lm)[np]}\left(\sqrt{k_{lm}/k_{np}} \pm \sqrt{k_{np}/k_{lm}}\right). \tag{12}$$

Here, the "$+(-)$" sign corresponds to the case where the two modes have phase velocities in the same (opposite) direction, k is the wavenumber in free space, k_{lm} and k_{np} are axial wavenumber of the two modes, and

TE $\rightarrow$ TE

$$\Xi^{\perp}_{[lm][np]} = \frac{a}{b}\frac{\zeta_{nl}x'_{lm}x'_{-np}\left\lfloor 2 - nl\left(1/x'^2_{lm} + 1/x'^2_{np}\right)\right\rfloor}{\sqrt{1 - l^2/x'^2_{lm}}\sqrt{1 - n^2/x'^2_{np}}\left(x'^2_{lm} - x'^2_{np}\right)^2}$$

$$\Xi^{\parallel}_{[lm][np]} = \begin{cases} 0, & nl = 0 \\ \Xi^{\perp}_{[lm][np]}, & \text{else} \end{cases} \tag{13}$$

$$\xi^{\perp}_{[lm][np]} = \frac{a}{b}\frac{\zeta_{nl}\left(x'^2_{-lm} + x'^2_{np} - 2nl\right)}{\sqrt{1 - l^2/x'^2_{lm}}\sqrt{1 - n^2/x'^2_{np}}\left(x'^2_{lm} - x'^2_{np}\right)^2}$$

$$\xi^{\parallel}_{[lm][np]} = \begin{cases} 0, & nl = 0 \\ \xi^{\perp}_{[lm][np]}, & \text{else} \end{cases} \tag{14}$$

TM → TM

$$\Xi^{\parallel}_{(lm)(np)} = \frac{a}{b}\frac{\zeta_{nl}\left(x_{lm}^2 + x_{np}^2\right)}{\left(x_{lm}^2 - x_{np}^2\right)^2}$$

$$\Xi^{\perp}_{(lm)(np)} = \begin{cases} 0, & nl = 0 \\ \Xi^{\parallel}_{(lm)(np)}, & \text{else} \end{cases} \tag{15}$$

$$\xi^{\parallel}_{(lm)(np)} = \frac{a}{b}\frac{\zeta_{nl} 2 x_{lm} x_{np}}{\left(x_{lm}^2 - x_{np}^2\right)^2}$$

$$\xi^{\perp}_{(lm)(np)} = \begin{cases} 0, & nl = 0 \\ \xi^{\parallel}_{(lm)(np)}, & \text{else} \end{cases} \tag{16}$$

TM → TE

$$\Xi^{\parallel}_{[lm](np)} = \frac{a}{b}\frac{\zeta_{nl} l}{\sqrt{x_{lm}'^2 - l^2}\left(x_{lm}'^2 - x_{np}^2\right)}$$

$$\Xi^{\perp}_{[lm](np)} = \begin{cases} a/\sqrt{2}\, b x_{0m}', & l = 0 \text{ and } m = p \\ \Xi^{\parallel}_{[lm](np)}, & nl \neq 0 \\ 0, & \text{else} \end{cases} \tag{17}$$

TM → TE

$$\Xi_{(lm)[np]} = \Xi_{[np](lm)} \tag{18}$$

where the radius of curvature is given by

$$b(z) = \frac{\left[1 + (ds/dz)^2\right]^{3/2}}{d^2 s/dz^2} \tag{19}$$

and

$$\zeta_{nl} = \sqrt{2/\varepsilon_{nl}} = \begin{cases} \sqrt{2}, & nl = 0 \\ 1, & \text{else.} \end{cases} \tag{20}$$

Note that (13)–(18) have been given in [8] for the perpendicular modes, but we have corrected an error that corresponds to (14). The fast-amplitude variation is integrated analytically, then the slow variation is integrated numerically via a predictor corrector method and the above equations [4].

An approximate formula for mode coupling when only two modes have nonzero amplitudes can be used to find a starting point for the waveguide dimensions. The beat wavelength is given by

$$\lambda_b = 2\pi \big/ \left|(k_{lm} - k_{np})\right|. \tag{21}$$

If we can write the coupling coefficient between the two modes of interest approximately as

$$\kappa_{\{lm\}\{np\}} \approx K_o \sin(2\pi z/\lambda_b) \tag{22}$$

we can find a requirement on K_o for total mode conversion [6]

$$K_o = \pi/(N\lambda_b). \tag{23}$$

The right-hand side of (23) is fixed, but the left-hand side depends on the ripple amplitude d

$$K_o \approx d(2\pi/\lambda_b)^2\left[1 - 0.75(2\pi d/\lambda_b)^2\right]K_o' \tag{24}$$

TABLE I
DIMENSIONS OF THE $TE_{12} \rightarrow TE_{01}$-MODE CONVERTER

Waveguide radius a (cm)	2.6035
Waveguide ripple d (cm)	0.0846
Period length λ_b (cm)	9.6300
Number of Periods N	7

where K_o' does not depend on the waveguide ripple and the approximation is good for small values of d/λ_b. For example, for the $TE_{12} \rightarrow TE_{01}$ converter, we can find

$$K_o' = \frac{x_{12}' x_{01}'\left[2a\left(k^2 + k_{12}k_{01}\right) - (x_{12}'^2 + x_{01}'^2)/a\right]}{\left[2k_{12}k_{01}\left(1 - 1/x_{12}'^2\right)\right]^{1/2}\left(x_{12}'^2 - x_{01}'^2\right)^2}. \tag{25}$$

Likewise, for the $TE_{11} \rightarrow TM_{01}$ converter, we can find

$$K_o' = \frac{ka\left(\sqrt{\frac{k_{01}}{k_{12}}} + \sqrt{\frac{k_{12}}{k_{01}}}\right)}{\sqrt{2\left(x_{11}'^2 - 1\right)}\left(x_{01}^2 - x_{11}'^2\right)}. \tag{26}$$

The design method entails picking a waveguide wall radius based on the application and selecting an N based on the length restrictions. Equations (21) and (24) are used to get initial guesses for λ_b and d. The numerical code is then iterated, making (usually) small changes in λ_b and d until the optimal results are obtained. If the mode conversion results are inadequate, the procedure is iterated with different values for N and a.

III. Simulation Results

A. $TE_{12} \rightarrow TE_{01}$-Mode Converter Design

The dimensions for the $TE_{12} \rightarrow TE_{01}$-mode converter design are given in Table I. Our studies indicate that the dependence of conversion efficiency on waveguide radius is weak near the nominal radius, thus, we choose it to correspond to WC205 waveguide to facilitate cold testing. A total of ten modes can exist in the waveguide at the designed operating frequency of 11.424 GHz. The cutoff frequencies of the TE_{01} and TE_{12} modes in WC205 are 7.05 and 9.77 GHz, respectively. Thus, a smaller waveguide radius could be utilized if converter length is a significant issue since the length for a given number of periods is reduced as the radius decreases because of the concomitant increase in the gap between the guide wavelengths of the two modes. The overall length of the converter is 67.41 cm. The ripple period is somewhat below the value 9.698 cm indicated by (21) and is found by maximizing the mode conversion. The ripple amplitude is exactly the same as predicted by the approximate solution and is only 3.25% of the waveguide radius.

The simulation results at the design point are given in Table II. The numbers represent the percentage of power in a particular mode at the end of the converter. For both polarizations, the TE_{12} mode is assumed to be incident on the converter entrance. There is no significant power reflected in any mode. Almost 98.5% of the TE_{12} power is converted into the TE_{01} mode when the converter is oriented as an H-plane bend. Less than 0.02% remains in the incident mode. The remaining 1.5% is divided

TABLE II
PERFORMANCE OF THE $TE_{12} \rightarrow TE_{01}$-MODE CONVERTER AT 11.424 GHz

Mode	% power at converter end	
	H-plane bend	E-plane bend
TE_{12}	0.016	98.904
TE_{01}	98.490	0.000
TE_{11}	1.009	0.001
TE_{21}	0.091	0.031
TE_{31}	0.003	0.003
TE_{41}	0.000	0.000
TM_{01}	0.000	0.010
TM_{02}	0.000	0.760
TM_{11}	0.293	0.043
TM_{21}	0.098	0.247

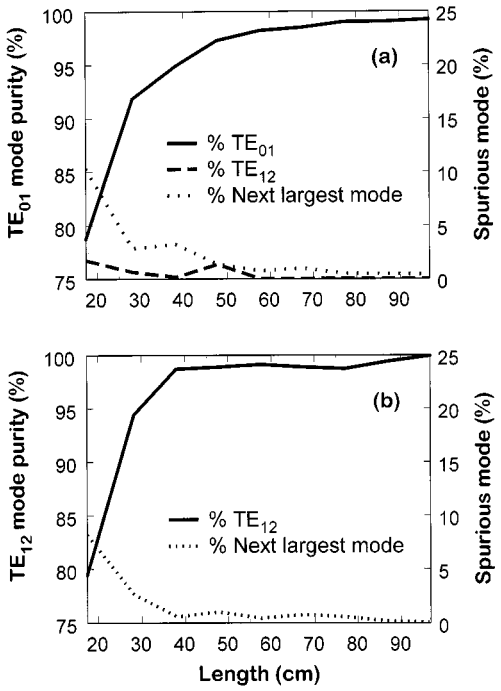

Fig. 2. Mode conversion as a function of length: (a) for H-plane orientation and (b) E-plane orientation at a frequency of 11.424 GHz for the $TE_{12} \rightarrow TE_{01}$ converter.

between a number of the other modes. The main spurious mode is the TE_{11} mode, which has about 1% of the incident power. This power undoubtedly comes from conversion of the TE_{01} power into TE_{11} power.

The division in power at the exit of the converter when it is oriented as an E-plane bend is also given in the table. Since there is no coupling to the TE_{01} mode in this orientation, the majority of the power remains in the TE_{12} mode (nearly 99%). The main spurious mode is the TM_{02} mode, which contains about 0.75% of the power. The only other mode to have significant power is the TM_{21} mode.

The number of periods was selected as a tradeoff between the need to have nearly complete mode conversion and the desire to have a short converter. The dependence of mode conversion at 11.424 GHz as a function of the number of periods (and, subsequently, the total length of the converter) is given in Fig. 2. For the H-plane orientation, the percentage of power converted to the TE_{01} mode drops off rapidly for lengths below 50 cm.

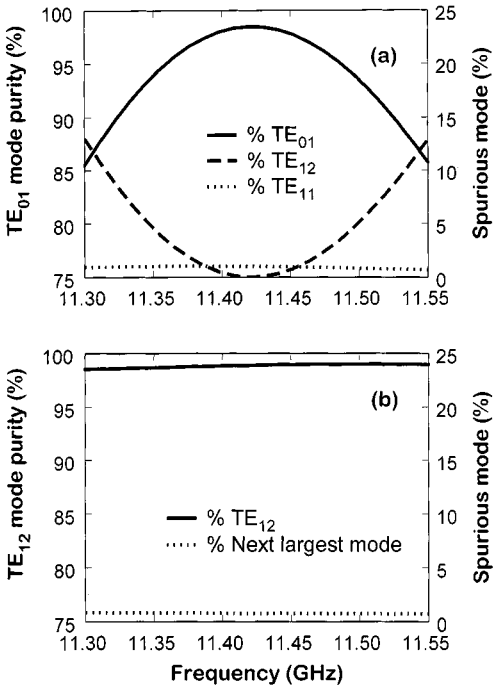

Fig. 3. Mode conversion as a function of frequency: (a) for H-plane orientation and (b) E-plane orientation for a seven-period $TE_{12} \rightarrow TE_{01}$ converter.

The main spurious mode is usually the TE_{11} mode, but for very short lengths, it could be the TM_{11} or TE_{21} mode. The residual amount of TE_{12} is negligible above 50 cm. The mode purity of the TE_{01} mode increases gradually to 99.23% at a length of nearly 1 m. For the E-plane orientation, spurious-mode conversion increases significantly as the length is decreased below 40 cm. The main spurious mode is usually the TM_{02} mode, but it is the TE_{21} mode for the shortest converter design. The TE_{12}-mode purity for the ten-period ($\sim$1 m) design is 99.95%.

Mode conversion as a function of frequency is plotted in Fig. 3 for the converter design given in Table I. Note that the spurious-mode conversion in the E-plane orientation is only weakly dependent on frequency. This is as expected because this mode conversion does not result primarily from a resonant effect. Likewise, the mode conversion in the H-plane orientation to the spurious TE_{11} mode is only weakly dependent on frequency. In contrast, the degree of mode conversion to the TE_{01} is very sensitive to frequency. If 95% mode conversion to the TE_{01} mode is acceptable, the bandwidth of the converter is about 130 MHz. The dependence of the ten-period ($\sim$1 m) design on frequency is shown in Fig. 4. Again, the spurious-mode conversion depends only weakly on frequency. The 95% bandwidth for this design is only 98 MHz. The reduced bandwidth is expected given the larger number of periods.

B. $TE_{11} \rightarrow TM_{01}$-*Mode Converter Design*

The dimensions for the $TE_{11} \rightarrow TM_{01}$-mode converter design are given in Table III. A 1-in-diameter waveguide is chosen for convenience. Only the TE_{11} and TM_{01} modes can exist at the designed operating frequency of 11.424 GHz, allowing the possibility for nearly complete mode conversion. The total length of the converter is about 1 m. The optimal ripple period is

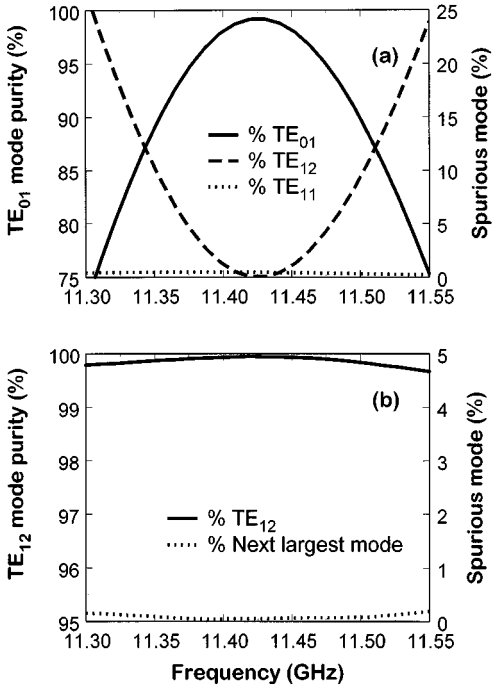

Fig. 4. Mode conversion as a function of frequency: (a) for H-plane orientation and (b) E-plane orientation for a ten-period $\mathrm{TE}_{12} \rightarrow \mathrm{TE}_{01}$ converter.

TABLE III
DIMENSIONS OF THE $\mathrm{TE}_{11} \rightarrow \mathrm{TM}_{01}$-MODE CONVERTER

Waveguide radius a (cm)	1.270
Waveguide ripple d (cm)	0.138
Period length λ_b (cm)	14.21
Number of Periods N	7

about 0.5% smaller than indicated by (21). The ripple height is exactly the same as predicted by the approximate solution and is about 11% of the waveguide radius.

The simulation results at the design point indicate that 99.999% of the power is converted from the TE_{11} mode into the TM_{01} mode. In fact, the mode conversion can be made to be essentially 100% efficient for converters with two or more periods. Fig. 5(a) shows the required ripple amplitude required for complete mode conversion (no more than 0.001% remaining in the TE_{11} mode) as a function of converter length. The left-most data point corresponds to two periods and the right-most point to seven periods. One assumption that is made to generate the coupling equations is that the radius of curvature b is large: $|a/b| \ll 1$. This assumption is valid even for the $N = 2$ case $(a/b < 0.33\%)$, although the large axis displacement may make fabrication difficult.

Mode conversion as a function of frequency is plotted in Fig. 5(b) for the $N = 3$ and $N = 7$ cases. The 95% bandwidth for the $N = 7$ case is about 180 MHz. The 95% bandwidth for the $N = 3$ case is over 400 MHz. There are no significant reflected waves for any of the designs.

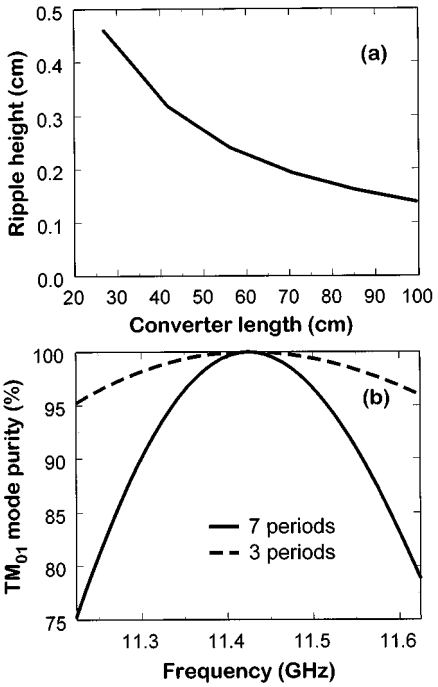

Fig. 5. $\mathrm{TE}_{11} \rightarrow \mathrm{TM}_{01}$ design. (a) Required ripple height as a function of length. (b) Mode conversion as a function of frequency for the three- and seven-period converters.

IV. EXPERIMENTAL VERIFICATION

The $\mathrm{TE}_{12} \rightarrow \mathrm{TE}_{01}$-mode converter was constructed and tested in our laboratory. The actual radius was reduced by about 2% due to a change in the specifications for the application, but the simulated results are virtually identical. The test consisted of measuring the radiation patterns from the mode converter in an anechoic chamber. The anechoic chamber used an open-ended X-band waveguide section as the pick-up antenna and could be swept to measure signals more than 40° above the center line of the converter. Two existing nonlinear tapers were used to bring the signal from the output of the converter to the 5-in-diameter aperture used by the anechoic chamber. According to simulations, the larger of the two tapers converted about 0.3% of the 11.424-GHz TE_{12} signal into the TE_{11} mode.

A scalar network analyzer was used to generate and measure the RF signal. A Marie converter was used to convert the signal in a rectangular guide into the TE_{01} mode. The measurement was complicated by the fact that the Marie converter produced small quantities of other modes, most noticeably the TE_{21} mode. To help compensate for this, the radiation patterns were measured at a number of different angular locations (relative to the rectangular guide orientation) and the results were averaged together. There were additional experimental errors related to the position measurement and the degree of polarization of the signal.

The averaged experimental radiation pattern for the Marie converter (when the serpentine converter was removed) is indicated by the crosses in Fig. 6. The theoretical curve is given by the solid line and is in excellent agreement with the measured results. The radiation patterns from the serpentine converter along

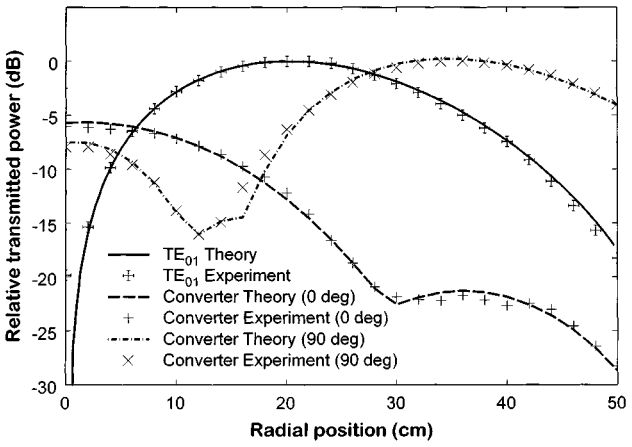

Fig. 6. Comparison of the theoretical and experimental far-field radiation patterns from the $\mathrm{TE}_{12} \rightarrow \mathrm{TE}_{01}$-mode converter.

lines perpendicular (0°) and parallel (90°) to the electric field are indicated by the "X" 's and "+" 's in Fig. 6, respectively. The fact that they do not converge to the same value on the center line is a manifestation of the measurement errors. The theoretical curves were generated by fixing the amplitudes of the dominant modes according to the simulations and then varying the phases to minimize the difference between the theory and measurements. Only the TE_{21} amplitude was allowed to vary since the content of that mode from the Marie converter is unknown. The resultant "best fit" TE_{21} amplitude was about 0.6%. The TE_{11} amplitude was set to 1.3% to account for the additional mode conversion in the nonlinear taper. The agreement between experiment and theory for both curves is excellent. Furthermore, the radiation patterns for distances greater than 30 cm from the center line are dominated by the TE_{12} pattern, and the relative agreement in those regions is excellent. Finally, only the TE_{1n} modes have a nonzero signal on the center line. The TE_{11} pattern is much stronger than the TE_{12} pattern there, so the relative powers in the TE_{11} and TE_{12} modes can accurately be discerned; we estimate that the relative power in the TE_{11} mode is, at most, 2% of the power in the TE_{12} mode.

V. Summary

In this paper, we have characterized the designs of two 11.424-GHz serpentine-mode converters, which have applications to HPM systems of current interest. We utilize several periodic perturbations in order to design tapers that have almost complete mode conversion between the two modes of interest, but minimal mode conversion between other modes. We have developed a simple approximate formula for the ripple amplitude d that has been proven in simulations to give nearly optimal mode conversion results. Both designs convert about 99% of the desired incident mode to the desired output mode when oriented appropriately, but have less than 1% mode conversion to all modes when oriented in the other polarization. Far-field radiation measurements of the TE_{12}-to-TE_{01}-mode converter support the theoretical predictions.

References

[1] M. Blank, K. Kreischer, and R. J. Temkin, "Theoretical and experimental investigation of a quasi-optical mode converter for a 110-GHz gyrotron," *IEEE Trans. Plasma Sci.*, vol. 24, pp. 1058–1066, June 1996.

[2] Z. D. Farkas, "Binary peak power multiplier and its application to linear accelerator design," *IEEE Trans. Microwave Theory Tech.*, vol. MTT–34, pp. 1036–1041, Oct. 1986.

[3] S. G. Tantawi *et al.*, "A multi-moded RF delay line distribution system for the next linear collider," in *Proc. 8th Workshop Advanced Accelerator Concepts*, July 1998, pp. 967–974.

[4] W. G. Lawson, "Theoretical evaluation of nonlinear tapers for a high-power gyrotron," *IEEE Trans. Microwave Theory Tech.*, vol. 38, pp. 1617–1622, Nov. 1990.

[5] ——, "Theoretical mode conversion in overmoded nonlinear coaxial waveguide tapers," *IEEE Trans. Microwave Theory Tech.*, vol. 42, pp. 127–131, Jan. 1994.

[6] C. Moeller, "Mode converters used in the Doublet III ECH microwave system," *Int. J. Electron.*, vol. 53, pp. 587–593, 1982.

[7] S. P. Morgan, "Theory of curved circular waveguide containing an inhomogeneous dielectric," *Bell Syst. Tech. J.*, vol. 36, pp. 1209–1251, 1957.

[8] E. Luneville, J.-M. Krieg, and E. Giguet, "An original approach to mode converter optimum design," *IEEE Trans. Microwave Theory Tech.*, vol. 46, pp. 1–9, Jan. 1998.

[9] J. S. McLean and R. J. Vernon, "A Design for a TE_{11}-to-TE_{01} serpentine mode converter for a Varian 7.2 GHz Klystron," Univ. Wisconsin, Madison, WI, Int. Rep., Mar. 10, 1992.

Wes Lawson (S'84–M'85–SM'96) received the B.S. degree in mathematics in 1980, and the B.S., M.S., and Ph.D. degrees in electrical engineering from the University of Maryland at College Park, in 1980, 1981, and 1985, respectively. His dissertation work involved theoretical and experimental studies of microwave generation in various large-orbit gyrotron configurations.

From 1978 to 1982, he was with the Electronic Systems Branch, Harry Diamond Laboratories. For the past 17 years, he has been with the Laboratory for Plasma Research, University of Maryland at College Park, where he is currently a Professor in the Department of Electrical Engineering. His principle interest lies in novel fast-wave microwave sources and his recent efforts have been directed toward high-power fast-wave and hybrid amplifiers and associated HPM components.

Melany R. Arjona was born in Panama City, Panama, in 1977. She is currently working toward the B.S. degree in electrical and computer engineering at the University of Maryland at College Park.

For the past three years she has been an Undergraduate Research Assistant with the Institute for Plasma Research, University of Maryland at College Park.

Bart P. Hogan was born in Bethesda, MD, on July 16, 1962. He received the B.S. degree in mechanical engineering from the University of Maryland at College Park, in 1986.

Since 1986, he has been with the Institute for Plasma Research, University of Maryland at College Park, where he is currently an Assistant Research Engineer. He is involved in a wide variety of projects in the field of HPM devices and components.

R. L. Ives (S'83–M'83–SM'93), photograph and biography not available at time of publication.